Monatsh Chem (2010) 141:691–697
DOI 10.1007/s00706-010-0262-z

ORIGINAL PAPER

Characterization of micrometer-sized magnetic optical sensor particles produced via spray-drying

Klaus Koren · Günter Mistlberger · Daniel Aigner · Sergey M. Borisov · Armin Zankel · Peter Pölt · Ingo Klimant

Received: 4 December 2009 / Accepted: 22 January 2010 / Published online: 19 February 2010

Abstract We investigated the correlation between optical sensing performance and morphology of micrometer-sized magnetic optical sensor particles (MOSePs). Oxygen-sensitive MOSePs were produced via spray-drying, a technique suitable for particle production from polymers in various solvents. A common problem of precipitation and polymerization techniques is the inhomogeneous distribution of dispersed nanoparticles. In spray-drying, this phenomenon is suppressed by fast solvent evaporation. The resulting sensor particles responded to changing analyte concentration within seconds, their Stern–Volmer calibration was highly linear, and they were magnetically controllable. The sensor characteristics resulted from the porosity of the matrix polymer, which enabled fast analyte diffusion towards the sensitive dye. Diffusion distances were further reduced by the formation of hollow particles. This was caused by the sequential drying of the polymer-solution droplet from the outside to the inside. Finally, the suitability of different polymers and magnetic nanoparticles for the production of MOSePs via spray-drying was evaluated.

Keywords Optical sensors · Electron microscopy · Magnetic particles · Fluorescence · Particles

K. Koren · G. Mistlberger (✉) · D. Aigner · S. M. Borisov · I. Klimant
Institute of Analytical Chemistry and Food Chemistry, Graz University of Technology, Graz, Austria
e-mail: mistlberger@tugraz.at

A. Zankel · P. Pölt
Austrian Centre for Electron Microscopy and Nanoanalysis, Institute for Electron Microscopy, Graz University of Technology, Graz, Austria

Introduction

Optical sensors are tools for monitoring analytes by correlating their concentration with light properties [1]. Since the introduction of optical sensors, they have constantly gained importance in industry and research laboratories [2]. Among others, physiologically important parameters such as oxygen and pH can be monitored using optical sensing systems [3]. For biological applications involving small objects of interest (e.g., cells, tissues or biofilms), miniaturized sensors are needed [4]. For this purpose, microoptodes and particle-based sensors are state of the art [5]. Micro- and nanometer-sized sensor particles have been produced using various polymerization methods, as well as grinding and precipitation techniques.

Recently, great efforts have been applied to the functionalization of nano- and microparticle-based sensors with magnetic particles, quantum dots, and antibodies [6]. The encapsulation of magnetic nanoparticles resulted in magnetically controllable optical sensor particles. As a result, novel applications of optical sensors (e.g., in situ sensor spot formation inside cultivation vessels or the formation of a "sensor swarm" [7, 8]) are possible.

In contrast to methods such as nanoprecipitation [9] and emulsion polymerization, spray-drying tolerates a variety of solvents, polymers, and additives. The composition of the obtained particles only depends on the mixture used for spraying. The rapid solvent evaporation suppresses inhomogeneities regarding the resulting nanoparticle distribution. The equipment required is cheap and simple (i.e., a conventional airbrush and a beaker). Spray-drying works without emulsifiers or other additives, which minimizes necessary purification steps. These aspects make spray-drying a straightforward concept towards micrometer-sized optical sensor particles.

Here, we present spray-drying as a versatile method for production of magnetic optical sensor particles (MOSePs). We report on the sensor characteristics and morphology of spray-dried magnetic optical sensor particles (sd-MOSePs). Comparing the sensor characteristics of sd-MOSePs with sensor films obtained by knife-coating demonstrated increased linearity of the Stern–Volmer correlation. The remarkable sensor characteristics are explained by detailed morphological studies.

Results and discussion

Oxygen-sensitive micrometer-sized particles consisting of poly(styrene-co-maleic anhydride) (PSMA), lipophilic magnetite nanoparticles (LMNPs), and cyclometalated iridium(III) coumarin complex ($Ir(Cs)_2(acac)$ [10]) were produced via spray-drying and subsequent hydrolysis of anhydride groups on the surface (Fig. 1). Spray-drying is a high-throughput method for polymer particle production. It tolerates different polymers, solvents, and additives such as inorganic nanoparticles. In contrast to most emulsion polymerization techniques, the produced particles are emulsifier free and, depending on the matrix polymer, ready to use right after production. Finally, the equipment required for spray-drying is simple and cheap, in the current case, an airbrush and a 10-dm^3 beaker.

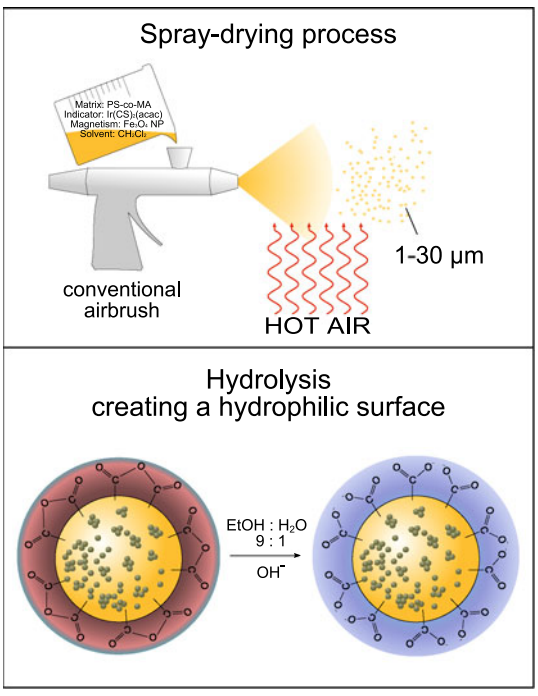

Fig. 1 Synthetic pathway towards micrometer-sized MOSePs. Polymer, indicator, and magnetite particles are dissolved and dispersed, respectively, in dichloromethane and are sprayed into a hot atmosphere using an airbrush. The obtained particles had sizes ranging from approximately 1 to 30 µm. Subsequent hydrolysis of the particles resulted in a hydrophilic surface

Prior to spraying, all components were dissolved and dispersed, respectively, in highly volatile dichloromethane. This mixture will be referred to as "cocktail" throughout the manuscript. The cocktail was nebulized through an airbrush into a preheated beaker. Upon contact with the hot gas phase, the cocktail droplets are transformed into particles due to rapid solvent evaporation. As previously reported [11], particles consisting of PSMA are dispersible in aqueous media due to the hydrophilic surface groups. The suitability of several polymers (Table 1) and LMNPs (Table 2) for spray-drying was tested. Particle morphology was characterized by scanning and transmission electron microscopy, and fluorescence and light microscopy, and sensor characteristics were determined by phase fluorimetric measurements at varying analyte concentrations.

Sensor characteristics

In contrast to the calibration plots observed for 5-µm-thick sensor films, spray-dried MOSePs showed a highly linear calibration behavior from $pO_2 = 0$ to 1,013 hPa (Fig. 2a).

Highly linear calibration curves are rare, especially for optical sensors with a working pO_2 range of 0–1,013 hPa. Nonlinear calibration curves can be explained by the so-called two-site model from Carraway et al. [12], suggesting that some dye molecules are less quenchable by the analyte than others. Therefore two different Stern–Volmer constants (K_{SV1} and K_{SV2}) and a distribution coefficient P are added to the classical Stern–Volmer equation.

$$\frac{\tau}{\tau_0} = \frac{P}{1 + K_{SV1} pO_2} + \frac{1 - P}{1 + K_{SV2} pO_2}.$$

This equation can be simplified by the assumption that one portion of the dye is virtually unquenchable, i.e., $K_{SV2} = 0$ [13].

$$\frac{\tau}{\tau_0} = \frac{P}{1 + K_{SV1} pO_2} + 1 - P.$$

Microheterogeneity of the polymeric matrix yields environments with different permeability and consequently different quenching behavior.

The Stern–Volmer constant K_{SV} decreased with increasing maleic anhydride content [10] (Table 1; Fig. 2a). The higher matrix polarity induced by maleic anhydride resulted in decreased lifetime of the indicator's excited state and consequently in decreased sensitivity. While the calibration curves of the sensor films are nonlinear (e.g., $R^2 = 0.969$), linear fits with $R^2 = 0.999$ or higher were obtained for the studied sd-MOSePs. Hence, the two-site model is required to fit the obtained curves ($R^2 > 0.998$). The estimated response time t_{90} (the time

Table 1 Applicability of polymers with varying maleic anhydride (MA) content and molecular weight (MW) for spray-drying

Polymer	MA (wt%)	MW (g mol^{-1})	Suitability for spray-drying		Sensor performance
PSMA93	7	224,000	+	++	0.00181
EF 80	11.11	14,400	+	+	0.00135
EF 60	14.29	11,500	+	−	NA
PSMA75	25	1,900	−	− −	NA
PS	0	220,000	NA	NA	0.0042

Table 2 Properties of magnetite nanoparticles (surface coating, dispersibility, and price) and their applicability for spray-drying

Magnetite type	Synthesis	Coating	Suitability for spray-drying	Price
CP-LMNP	Coprecipitation	Oleic acid	++	++
TD-LMNP	Thermal decomp.	Oleic acid	+	+
EMG1200	Commercial	Fatty acid	+	−
EMG1300	Commercial	Polymeric	++	−
EMG1400	Commercial	Hydrophobic	−	−

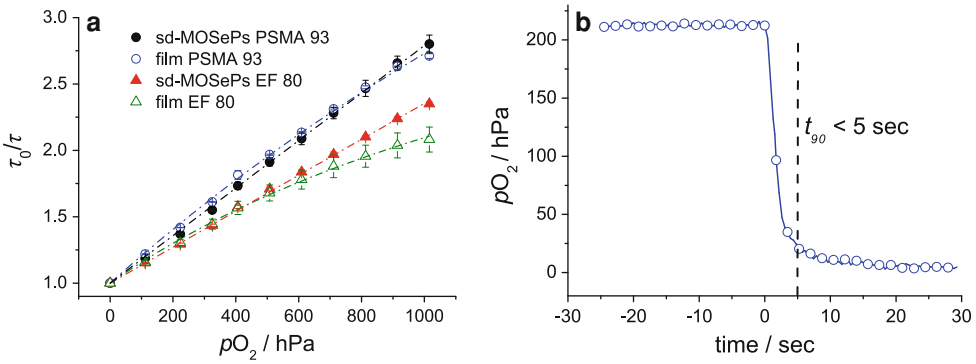

Fig. 2 **a** Comparison of the calibration curves (Stern–Volmer plots) of 5-µm-thick sensor films and spray-dried particles. While the calibration curves of the sensor films were fitted using the two-site model, sensor particles (10 mg_{Poly}/g_{Solv}; 100 mg_{Mag}/g_{Poly}) showed a highly linear Stern–Volmer correlation. K_{SV} values decreased with increasing polarity of the matrix. **b** The response time of the MOSePs to changing oxygen concentration is fast enough for monitoring most biological processes ($t_{90} < 5$ s)

required to achieve 90% of the signal change) is less than 5 s (Fig. 2b), which is sufficiently fast for measurements of most biological growth processes.

As demonstrated below, structural investigations explain this unexpectedly high linearity of the sd-MOSePs calibration curves.

Fluorescence and light microscopy

Particle specific surface area and dimensions dramatically influence analyte diffusion towards the sensitive dye. Therefore, we determined the size distribution of the produced particles based on light and fluorescence microscopy images. Figure 3 shows polydisperse particles with sizes ranging from 1 to 30 µm. Although uniform particles are beneficial for certain applications, monodispersity is usually not essential. As shown here, the performance of MOSePs in oxygen monitoring is unaffected by the different particle sizes. The reason is the unique matrix structure, as described in the following section.

Furthermore, not all the observed particles were perfectly spherical and the luminescence intensity was not equally distributed over the entire particle. Assuming a homogeneous distribution of the indicator dye in the polymeric matrix, the high luminescence intensities at the edges indicate a hollow particle structure. However, the same effect might have resulted from an inhomogeneous distribution of the dye in the particle. Therefore, the particle morphology was further investigated by electron microscopy.

Scanning electron microscopy

The scanning electron microscopy (SEM) images in Fig. 4a indicate a porous surface structure of the particles. A nanoporous structure favors short response times

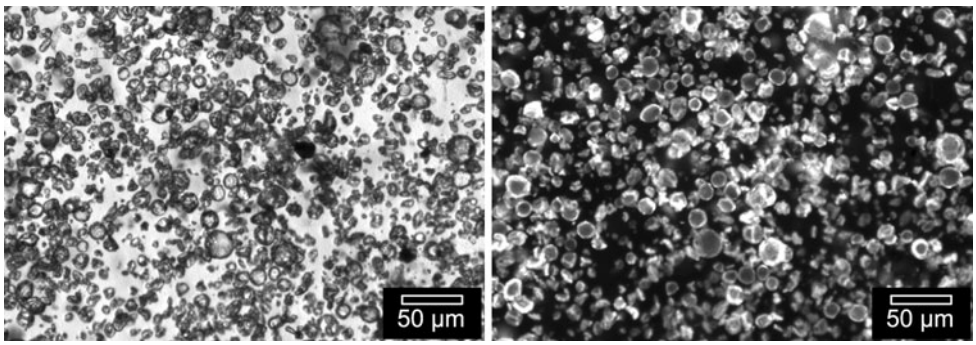

Fig. 3 Light (*left*) and fluorescence (*right*) microscopy images of sd-MOSePs (20 mg_{Poly}/g_{Solv} PSMA93; 300 mg_{Mag}/g_{Poly} LMNP) indicate a broad size distribution with average diameter of 5–7 µm

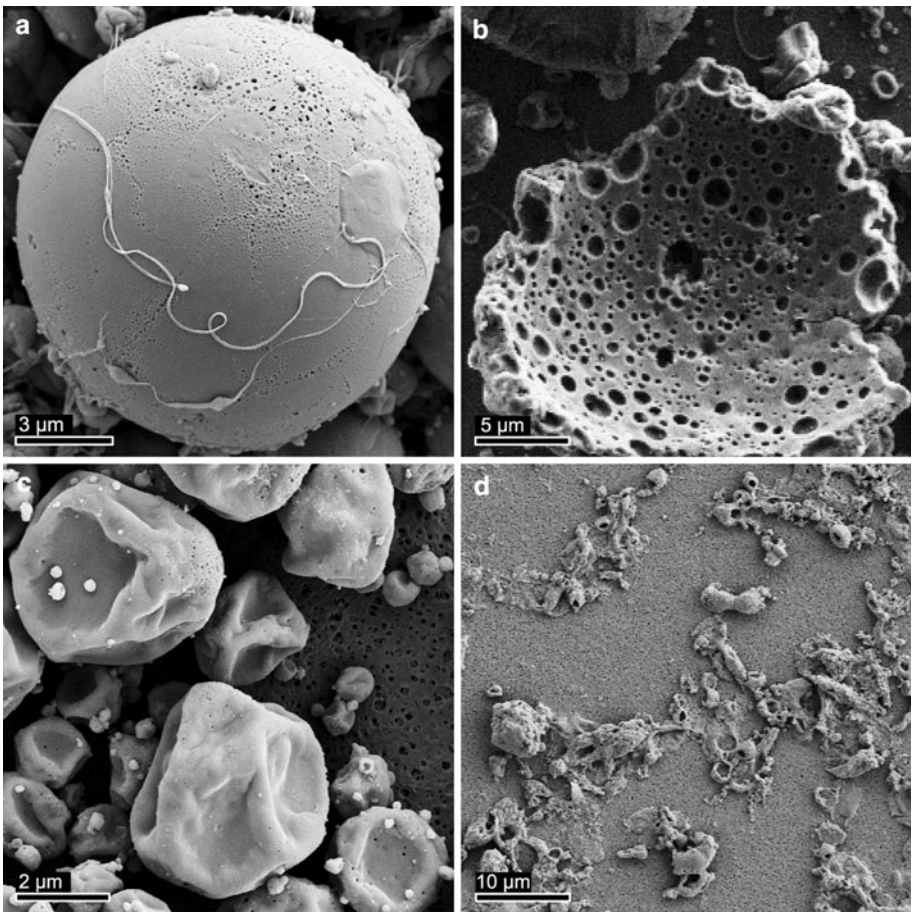

Fig. 4 SEM images of different sd-MOSePs (all particles with 20 mg_{Poly}/g_{Solv} and 300 mg_{Mag}/g_{Poly} LMNP). **a** Spherical particles with a nanoporous matrix were obtained using PSMA93. **b** The porous shell structure is seen in a particle fragment (PSMA93). **c** Low-molecular-weight polymers (EF80 and EF60) yielded partly collapsed, nonspherical particles. **d** No particles were found when using the polar, low-molecular-weight matrix PSMA75

because of decreased analyte diffusion distances. The average diameter of the pores of the particle in Fig. 4a was 160 ± 60 nm. The fragment of a broken sensor sphere depicted in Fig. 4b gives deeper insight into the structure of sd-MOSePs. Firstly, the spheres were obviously hollow, and secondly the pores seemed to penetrate the polymeric shell connecting the outside with the hollow particle core. These morphological features are important and explain both the sensor characteristics and the particle formation steps.

The particle formation process can be separated into three steps: (1) the shear gas stream forms cocktail droplets at the nozzle of the airbrush and ensures rapid transport of the droplets to the hot gas phase in the beaker. (2) Temperatures above the solvent's boiling point and the high vapor pressure of the solvent ensure fast drying around the outside of the droplets. Thereby, a solid polymer film encloses the cocktail droplets. (3) During sequential drying from the outside to the inside, the solvent disrupts the outer polymer shell, forming pores. In this final phase, the cocktail components precipitate and stick to the initially formed polymer film. Depending on the polymer properties and the rigidity of the initial outer layer, the spheres either keep their spherical shape and initial droplet diameter

(Fig. 4a) or collapse during phase 3. The result is a folded structure similar to a compressed paper bag (Fig. 4c). The molecular weight of the polymer is a crucial factor for the rigidity of the initial shell. The tendency of the spheres to collapse during phase 3 increased with decreasing molecular weight (MW) of the tested polymers, as can be seen in Figs. 4a (MW = 224,000 g mol^{-1}) and 4c (MW = 14,400 g mol^{-1}).

The SEM images reveal the porous structure of sd-MOSePs and suggest a hollow particle core. However, they do not provide insight into the distribution of pores and magnetite in the shell. In addition, the shell thickness remains unknown. This information is available from TEM images of a particle's thin section achieved by ultramicrotomy.

Transmission electron microscopy

Sectioning of particles by ultramicrotomy enabled visualization of the particle interior via TEM. A cross-section through an sd-MOSeP is shown in Fig. 5. This image confirms the assumption of a structure with a hollow core and a polymeric shell. A particle of 28 µm diameter is relatively large, and a bulk sensor with this thickness responds slowly to changing analyte concentration. However, the thin shell of the particle reduces diffusion distances and consequently the sensor's response time. The

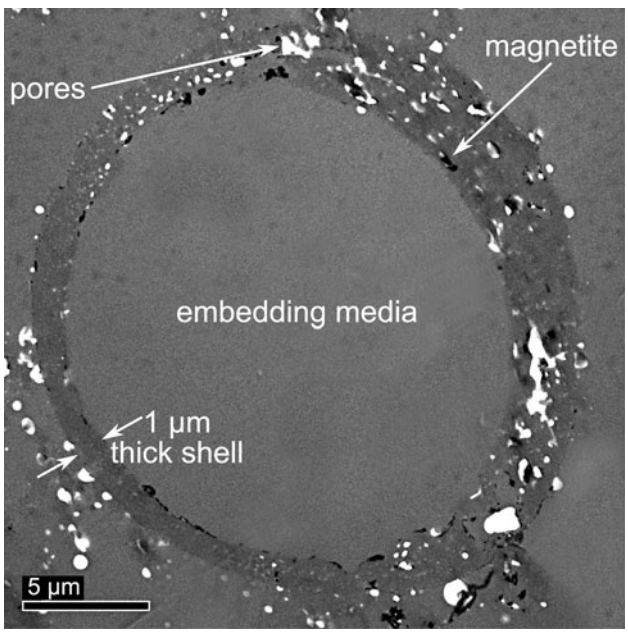

Fig. 5 TEM image of a thin-sectioned particle (20 mg_{Poly}/g_{Solv} PSMA93; 300 mg_{Mag}/g_{Poly} LMNP) indicates a hollow structure. Magnetite particles aggregate inside the polymeric shell (*black regions*). While the particle diameter is 28 µm, the polymeric shell is only 1–4 µm thick. Analyte diffusion towards the sensitive dye is favored by the porous structure (*white holes*)

shell thickness in sd-MOSePs is usually ~1/10 of the particle diameter (e.g., 1–4 µm in Fig. 5). Moreover, the thickness of the shell reveals the ratio between pores and bulk material of the particle. The pore volume in the shell can be estimated with the following assumption. Based on the particle formation process outlined above, the particle diameter should be roughly constant during the drying process ($d_{Particle} = d_{Droplet}$). In this case, the pore ratio R in percent can be calculated by

$$R = 1 - \frac{d^3 c}{\rho(d^3 - (d - 2t)^3)} \times 100,$$

where d is the droplet diameter, c is the concentration of the solids in the cocktail in kg m^{-3}, ρ is the average density of the solid phase, and t is the shell's thickness. The evaluation of this equation for the particle shown in Fig. 5 results in a pore fraction in the shell of more than 95%. Even if 80% of the solvent evaporates before the particle reaches its final size, the pore fraction is still approximately 80%. Such a high porosity further decreases diffusion distances and response times. Analyte diffusion, a common factor limiting the response time of optical sensors, is very fast in a material with high specific surface area and thin bulk structures.

Moreover, the porous structure provides an explanation for the linear Stern–Volmer correlation. Due to the high porosity, the polymer structure is amorphous since thin polymeric layers can hardly crystallize. Microheterogeneities resulting in varying permeability are therefore prevented, and all indicator molecules are equally accessible for the analyte.

Finally, TEM revealed the structure of the magnetic nanoparticles in the matrix polymer. The black regions inside the polymeric shell (Fig. 5) originate from magnetite aggregates. During the drying of the particles, the lipophilic magnetic nanoparticles change from a homogeneous dispersion in the cocktail to an aggregated state in the final particles. This might cause the inhomogeneous magnetite distribution over the particle population. However, aggregation also reduces the contact surface between magnetite and luminophore. As a result, luminescence quenching and the inner filter effect are minimized and this increases the signal intensity.

Material studies

The preparation of sd-MOSePs was successful using three different polymers and four different LMNPs. The most hydrophilic PSMA75 with the smallest molecular weight (1,900 g mol^{-1}) yielded aggregates rather than defined particles (Fig. 4d). Due to the low molecular weight the matrix structure was less stable and the high polarity caused partial solubility in the alkaline EtOH/water

hydrolysis medium. The trend that low-molecular-weight polymers formed less stable structures was supported by the EF60 and EF80 results. Spraying cocktails with these matrix polymers resulted in collapsed spheres (Fig. 4c). On the contrary, particles from PSMA93, the polymer with the highest molecular weight in this study, retained the spherical shape of the droplet with a hollow core (Figs. 4a, 5).

The suitability of a polymer for particle formation is necessary but not sufficient for applicable optical sensor particles. In order to achieve water-dispersible sensor particles a substantially hydrophilic surface is required. This is achieved by polar matrix groups (maleic anhydride) that are hydrolyzed to carboxyl groups after particle formation. On the other hand, strong hydrophobic interactions between the nonpolar indicator dyes and the matrix are required. While both EF80 (11.1 wt% MA) and EF60 (14.3 wt% MA) yielded particles, only EF80 was suitable for production of MOSePs. In case of EF60, the polarity was too high to keep the $Ir(Cs)_2acac$—the oxygen-sensitive dye—inside the matrix. As a consequence, the dye leached out into the ethanolic hydrolysis medium and the final particles were virtually nonluminescent.

The influence of the polymer concentration in the cocktail on the particle size and structure was also studied. A 10 mg polymer per gram solvent (mg_{Poly}/g_{Solv}) cocktail was optimal for the production of sensor particles. Higher concentrations ($\geq$20 mg_{Poly}/g_{Solv})—especially of high-molecular-weight polymers—favored aggregation and fiber-like structures. Lower concentrations increased the solvent consumption without significant impact on particle size (Table 3). As mentioned above, the spray-drying process is versatile and suitable for different classes of polymers and molecular weights. However, the cocktail composition requires optimization for each new polymer–solvent system. Hence, it is difficult to propose a universal recipe.

In addition, three commercial and two self-prepared LMNPs were tested for sd-MOSePs. The most important property of the LMNPs was good dispersibility in the solvent, here dichloromethane. The dispersibility decreased from EMG1300 (perfectly dispersible) to EMG1200, TD-LMNP, and CP-LMNP (dispersible in smaller concentrations), and finally to EMG1400, which was not dispersible at all. CP-LMNPs were prepared by coprecipitation followed by surface coating with oleic acid [14]. Thermal decomposition of Fe oleate also yielded magnetic nanoparticles (TD-LMNP) [15]. A key problem of the latter method was the presence of strongly attached organic impurities which represented the main component of the resulting precipitate. Although both self-made LMNPs were successfully incorporated into sd-MOSePs, the current study was carried out with commercial EMG1300 to ensure highest reproducibility of the results.

The LMNP content in the cocktail accounts for the magnetic separability of the resulting sensor spheres. Higher magnetite content results in faster response to a changing magnetic field and in the strong attachment to a magnetic separator. On the contrary, the dark magnetite efficiently absorbs light from both excitation and luminescent emission and therefore decreases the signal intensity. As a result, the concentration required optimization and we found 100 mg per gram polymer (mg_{Mag}/g_{Poly}) to be a good trade-off between magnetic separability and optical signal intensity. The filter effect of magnetite caused a 50% signal reduction when increasing the concentration from 100 mg_{Mag}/g_{Poly} to 300 mg_{Mag}/g_{Poly}. A concentration below 100 mg_{Mag}/g_{Poly} reduced the particle yield during washing due to low collection efficiency.

Sensor stability and measurement reproducibility are important factors regarding the applicability of an optical sensor. The performance of the spray-dried particles presented herein did not change after several months of storage in the dark. This indicates that the structure of the particles did not change over time. Nonetheless it has to be mentioned that bleaching of the indicator dye occurs. Dye bleaching is the only process affecting the sensor stability and performance over time [10]. This problem might be overcome by using dyes with increased photostability.

Table 3 Size distribution d (from light microscopy) of sprayed particles with different polymers and polymer concentrations c in the cocktail

Polymer	c (mg_{Poly}/g_{Solv})	d ($\pm s$) (μm)
PSMA93	5	5 (±2)
PSMA93	10	7 (±3)
PSMA93	20	6 (±3)
EF80	5	7 (±2)
EF80	20	5 (±3)

Conclusion

We present spray-drying as a versatile and straightforward method to produce magnetic polymer microparticles with optical sensor properties. Starting from a dispersion and solution, respectively, of all desired compounds in a volatile solvent, the sensor particles were formed directly and without emulsifier. Compared with other particle production methods, spray-drying is highly flexible regarding polymers, solvents, and additives in the cocktail. The oxygen-sensitive sd-MOSePs displayed a linear Stern–Volmer correlation from $pO_2 = 0$ to 1,013 hPa, a rare property of optical oxygen sensors. Morphological studies

revealed the reason for this linearity. The particles were found to be hollow and to contain a thin shell which was highly porous. This led to fast responding sensors and finally ensured that all indicator molecules were located in the same environment, explaining the linear calibration curves.

Materials and methods

Materials

Polystyrene (PS) and poly(styrene-co-maleic anhydride) (PSMA) polymers were purchased from different suppliers: PSMA93 and PS from Sigma–Aldrich, both EF80 and EF60 from Sartomer (www.sartomer.com), and PSMA75 from Scientific Polymers (www.scientificpolymer.com). Sodium hydroxide, dichloromethane, and ethanol were purchased from Carl Roth (www.carl-roth.de). Magnetite nanoparticles were either prepared by thermal decomposition [15] or coprecipitation followed by surface modification [14]. The Nanoparticle Developer Kit including EMG1200, EMG1300, and EMG1400 was purchased from FerroTec, Inc. (www.ferrotec.de). The O_2-sensitive dye $Ir(Cs)_2(acac)$ was prepared in our laboratory as described elsewhere [10]. Oxygen and nitrogen were of 99.999% purity and purchased from Air Liquide (www.airliquide.at).

Particle production

MOSePs were prepared using a spray-drying process. Typically, 100 mg polymer and 1.5 mg $Ir(Cs)_2(acac)$ were dissolved in 10 g dichloromethane. Magnetite nanoparticles (10 mg) were added to the solution and dispersed by sonication. This cocktail was sprayed into a preheated 10-dm^3 glass beaker using a conventional airbrush (HP 120 with nozzle diameter of 0.2 mm, www.conrad.at). After spraying, the particles were dispersed in 100 cm^3 ethanol. Then 10 cm^3 of a 10 M NaOH solution were added to hydrolyze the anhydride groups on the surface under sonication for 15 min. The MOSePs were magnetically separated and washed with water until neutral. The particles were redispersed in water to final concentration of 10 mg cm^{-3}.

Sensor characterization

The sensor characteristics of oxygen-sensitive MOSePs were investigated using a phase fluorimeter (pH-Mini, PreSens GmbH, Germany). The modulation frequency was adjusted to 20 kHz. The sensor particles were collected in front of an optical fiber with the help of a specialized magnetic separator [16]. Different ratios of oxygen and nitrogen required for the calibration were adjusted with a gas mixing device (MKS, www.mksinst.com). As reference, 5-µm-thick PSMA films containing 1.5 wt% $Ir(Cs)_2(acac)$ were used.

Microscopy

Light-microscopic images were acquired using a PCO SensiCam (PCO Computer Optics GmbH, Kelheim, Germany) digital camera mounted onto a Zeiss (Göttingen, Germany) Axiovert 25 CFL inverted fluorescence microscope. SEM images were collected using a Zeiss Ultra55 microscope (www.smt.zeiss.com). The particles were dried on a polymeric support [polytetrafluoroethylene (PTFE) filter membrane] and sputtered with Au/Pd. For TEM investigations MOSePs were embedded and cut using ultramicrotomy. TEM images were collected at a Tecnai 12 transmission electron microscope (www.fei.com).

Acknowledgments The authors thank S. Fladischer, C. Mayrhofer, and E. Ingolic from the Austrian Centre for Electron Microscopy and Nanoanalysis for their technical support.

References

1. McDonagh C, Burke CS, MacCraith BD (2008) Chem Rev 108:400
2. Wolfbeis OS (2008) Anal Chem 80:4269
3. Wolfbeis OS (2005) J Mater Chem 15:2657
4. Klimant I, Kuehl M, Glud RN, Holst G (1997) Sens Actuators B 38:29
5. Borisov SM, Mayr T, Klimant I (2008) Anal Chem 80:573
6. Borisov SM, Klimant I (2008) Analyst 133:1302
7. Anker JN, Koo YE, Kopelman R (2007) Sens Actuators B121:83
8. Chojnacki P, Mistlberger G, Klimant I (2007) Angew Chem Int Ed 46:8850
9. Borisov SM, Mayr T, Mistlberger G, Waich K, Koren K, Chojnacki P, Klimant I (2009) Talanta 79:1322
10. Borisov SM, Klimant I (2007) Anal Chem 79:7501
11. Mistlberger G, Borisov SM, Klimant I (2009) Sens Actuators B 139:174
12. Carraway ER, Demas JN, DeGraff BA, Bacon JR (1991) Anal Chem 63:337
13. Klimant I, Ruckruh F, Liebsch G, Stangelmayer A, Wolfbeis OS (1999) Mikrochim Acta 131:35
14. Ramírez LP, Landfester K (2003) Macromol Chem Phys 204:22
15. Park J, An K, Hwang Y, Park JG, Noh HJ, Kim JY, Park JH, Hwang NM, Hyeon T (2004) Nat Mater 3:891
16. Mistlberger G, Chojnacki P, Klimant I (2008) J Phys D Appl Phys 41:085003